Effect of Pressure on Proton-Transfer Rate from a Photoacid to Ethanol Solution

Nahum Koifman, Boiko Cohen, and Dan Huppert*

Raymond and Beverly Sackler Faculty of Exact Sciences, School of Chemistry, Tel Aviv University, Tel Aviv 69978, Israel

Received: November 12, 2001; In Final Form: January 30, 2002

The reversible proton dissociation and geminate recombination of photoacids is studied as a function of pressure in liquid ethanol. For this purpose, we used a strong photoacid, 5,8-dicyano-2-naphthol (DCN2) ($pK_a^* \approx -4.5$ in water), capable of transferring a proton to alcohols. The time-resolved experimental data are explained by the reversible diffusion-influenced chemical reaction model. At low pressure, the proton-transfer rate increases with pressure, while at high pressure, the rate constant decreases as the pressure increases. The pressure dependence is explained using an approximate stepwise two-coordinate proton-transfer model. The model is compared with the Landau−Zener curve-crossing proton-tunneling formulation. Decrease of the proton-transfer rate at high pressures denotes the adiabatic limit, while the increase in rate at low pressures denotes the nonadiabatic limit.

Introduction

To understand the dynamics of intermolecular proton transfer in clusters in the liquid phase[1−4] and the solid state,[5−9] a large effort has been made over the past 4 decades. The phenomenon of excited-state proton transfer (ESPT) from a photoacid molecule, which dissociates upon excitation to produce an excited anion and a proton,[10−13] was used in time-resolved studies in liquids. Recent studies[1,3,14−17] emphasize the dual role played by the solvent molecule (1) as proton acceptor and (2) as a solvating medium of both the reactant and the product.[18−20]

Theories of proton tunneling in chemistry are based on the work of Bell.[21,22] The evidence of tunneling is taken to be a large kinetic isotope effect (KIE) and the concave-curved non-Arrhenius behavior of log(*k*) vs 1/*T*, that is, at low temperatures the proton/deuteron transfer rate constant exhibits a smaller temperature dependence.

More recent theories have revealed that tunneling is the dominant reaction mode for proton transfer, even at ambient temperatures. The theory of the proton-transfer reaction in solution was developed by Dogonadze, Kuznetzov, Ulstrup, and co-workers[23,24] and then extended by Borgis and Hynes, Cukier, and Voth.[25−27] These theories show that the presence of a potential energy barrier in the proton-reaction coordinate causes tunneling through the barrier in the reaction pathway, as opposed to passage over barrier. The theory of proton-transfer tunneling in solids was summarized in ref 9.

In recent papers,[14−17] we described our experimental results of an unusual temperature dependence of excited-state proton transfer from a super photoacid (5,8-dicyano-2-naphthol, DCN2) to liquid monols, diols, and glycerol. In methanol and ethanol at temperatures above 285 K, the rate of the proton transfer is almost temperature-independent, while at $T < 250$ K, the rate exhibits great temperature dependence. The rate constant is similar to the inverse of the longest component of the dielectric relaxation time of a particular protic solvent. We proposed a simple stepwise model to describe and calculate the temperature dependence of the proton transfer to the solvent reaction. The model accounts for the large difference in the temperature dependence and the proton-transfer rate at high and low temperatures and the solvent dependencies.

The unusual temperature dependence is explained using proton-transfer theory, based on the Landau−Zener curve-crossing formulation. The high-temperature behavior of the rate constant denotes the nonadiabatic limit, while the low-temperature behavior denotes the adiabatic limit. We used an approximate expression for the proton-transfer rate, which bridges the nonadiabatic and the solvent-controlled adiabatic limit, to fit the temperature-dependence curve of the experimental proton-transfer rate constant.

In the condensed phase, pressure is known to influence chemical-reaction rates. External pressure changes such properties of the medium and reactants as reaction free volume, the potential-energy profile along the reaction path, compressibility, viscosity, and the energy of reorganization of the medium.[8] The absolute value of the reaction rate constant and its temperature dependence can depend on all of these parameters. The pressure influences both the characteristics of classical over-barrier reactions and those of the tunneling transfer of the proton. The pressure influence on tunneling in the solid state is discussed in detail in refs 8 and 9. In solids, the tunneling reaction depends exponentially on both the equilibrium distance between the reactants and the frequency of intermolecular vibrations, which vary with compression.

Time-resolved picosecond fluorescence studies of excited aqueous 8-hydroxy-1,3,6-pyrene trisulfonate (HPTS) have been carried out at pressures up to the ice transition point of H_2O and D_2O.[28] The proton-transfer rates derived from these studies exhibit a linear increase with pressure from 8×10^9 s^{-1} at 1 atm and 294 K to 2.5×10^{10} s^{-1} at the liquid → ice VI transition point at 9 kbar and 294 K. In D_2O, the deuteron-transfer rate also increases linearly with pressure from 2.7×10^9 s^{-1} at 1 atm to 1×10^{10} s^{-1} at 8 kbar. The low-pressure isotope effect, $k_{H^+}/k_{D^+} \cong 3$, is maintained across the pressure range studied. From these results, an activation volume, $\Delta V_0^{\ddagger}$ of -6 cm^3/mol is obtained.

* To whom correspondence should be addressed. E-mail: huppert@tulip.tau.ac.il. Fax/phone: 972-3-6407012.

10.1021/jp0141427 CCC: $22.00
Published on Web 04/09/2002

In this paper, we study the effect of pressure on the dynamics of excited-state intermolecular proton transfer (ESPIT) from DCN2 to ethanol. The main finding of this study is that at low pressure (up to ~10 kbar) the proton-transfer rate increases while at high pressure (10−20 kbar) the proton-transfer rate decreases with pressure. The experimental data are explained by our stepwise model that can be related to the Dogonadze−Kuznetzov[23] and Borgis−Hynes[25] theories of proton transfer, both based on the Landau−Zener curve-crossing formulation.

Experimental Section

Pressurized time-resolved emission was measured in a compact gasketed diamond anvil cell[29] (DAC) purchased from D'Anvil[30,31] with 0.3 carat low-fluorescent high-UV transmission diamonds. To provide a larger volume of the sample for sufficient fluorescent intensity, a 1 mm hole was drilled in the 1 mm thick stainless gasket. The low-fluorescence-type diamonds served as anvils. The anvil seats had suitable circular apertures for the entry and exit of the exciting laser beam and the excited fluorescent intensity. With this cell, pressures up to 30 kbar were reached without detriment to the diamond anvils. The pressure generated was calibrated using the well-known ruby fluorescent technique.[32]

Time-resolved fluorescence was measured using the time-correlated single-photon counting (TCSPC) technique. As an excitation source, we used a cw mode-locked Nd:YAG-pumped dye laser (Coherent Nd:YAG Antares and a 702 dye laser), providing a high repetition rate (>1 MHz) of short pulses (2 ps at full width half-maximum, fwhm). The TCSPC detection system is based on a Hamamatsu 3809U photomultiplier, Tennelec 864 TAC, Tennelec 454 discriminator, and personal computer-based multichannel analyzer (nucleus PCA-II). The overall instrumental response was about 50 ps (fwhm). Measurements were taken at 10 nm spectral width. Steady-state fluorescence spectra were taken using a SLM AMINCO-Bowman-2 spectrofluorometer.

DCN2 was synthesized by Tolbert and co-workers.[33] The sample concentrations were between 4×10^{-4} and 1×10^{-4} M. Solvents were of reagent grade and were used without further purification. The solution's pH was approximately 6.

The DCN2 fluorescence spectrum consists of two structureless broad bands (~40 nm fwhm). The emission band maximum of the acidic form (ROH*) in water and in alcohols emits at 450 nm. The emission band maximum of the alkaline form (RO^-*) in water and in alcohols emits at 600 nm. At 450 nm, the overlap of the two luminescence bands is rather small and the contribution of the RO^-* band to the total intensity at 450 nm is about 1%. In addition, we find that some fluorescent impurity in the DCN2 compound emits in the UV and blue part of the emission spectrum. At 1 atm, the impurity emission level is about 1% of the peak intensity at 450 nm, and it increases up to 4% at 20 kbar. The pressure dependence of the background luminescence can arise from dimerization of DCN2 to a non-proton-emitting dimer. Therefore, in the time-resolved analysis, we add to the calculated signal an additional component with an exponential decay of 10 ns with an amplitude of about 2% at 1 atm, which increases with pressure up to 4% at 20 kbar, to account for the impurity fluorescence. To avoid ambiguity due to the overlap between the fluorescence contributions of ROH* and RO^-* and to minimize the impurity fluorescence, we mainly monitored the ROH* fluorescence at 470 nm.

Results

Reversible Diffusion-Influenced Two-Step Model. Experimental and theoretical studies of reversible ESPT processes in solution have led to the development of a reversible diffusion-influenced two-step model[34,35] (Scheme 1). The first step is described by back-reaction boundary conditions with intrinsic rate constants k_{PT} and k_r. This is followed by a diffusion second step in which the hydrated proton is removed from the parent molecule. This latter step is described by the Debye−Smoluchowski equation (DSE). In the continuous diffusion approach, the photoacid dissociation reaction is described by the spherically symmetric diffusion equation (DSE)[36] in three dimensions.[34,35] The boundary conditions at $r = a$ are those of the back reaction (Scheme 1). The parameters k_{PT} and k_r are the "intrinsic" dissociation and recombination rate constants at the contact sphere radius a. Quantitative agreement was obtained between theory and experiment,[34,35] and as a result, it was possible to make a closer study of the influence of the dynamic and static properties of the solvent on the ESPT process. A detailed description of the model as well as the fitting procedure is given in refs 14, 34, and 35.

SCHEME 1

$$ROH^* \underset{k_r}{\overset{k_{PT}}{\rightleftharpoons}} [RO^-{}^* \ldots H^+]_{(r=a)} \overset{DSE}{\rightleftharpoons} RO^-{}^* + H^+$$

The comparison of the numerical solution with the experimental results involves several parameters. Some are adjustable parameters, like k_{PT} and k_r, while others, like the contact radius, a, have acceptable literature values.[34,35] The proton-dissociation rate constant, k_{PT}, is determined from the exponential decay at early times of the fluorescence decay. At longer times, the fluorescence decay is nonexponential because of the reversible geminate recombination.

An important parameter in our model that strongly influences the nonexponential decay is the mutual diffusion coefficient, $D = D_{H^+} + D_{RO^-}$. The pressure dependence of the proton-diffusion constant, D_{H^+}, for ethanol as a function of pressure is unknown but can be roughly estimated from the viscosity dependence on pressure.[37] At 1 atm, it was calculated from the proton-conductance measurements.[38] The anion diffusion constant, D_{RO^-}, as a function of pressure was estimated from the solvent viscosity dependence on pressure data.[39] Figure 1a shows the viscosity dependence on pressure of ethanol at 303 K taken from ref 37. The log of the viscosity increases at low pressures linearly with the pressure. At high pressure (>8 kbar), the slope decreases. Another important parameter in the model is the Coulomb potential between the anion, RO^-*, and the geminate proton.

$$V(r) = -\frac{R_D}{r}; \quad R_D = \frac{|z_1 z_2| e^2}{\epsilon k_B T} \tag{1}$$

R_D is the Debye radius, z_1 and z_2 are the charges of the proton and anion, ϵ is the static dielectric constant of the solvent, T is the absolute temperature, e is the electronic charge, and k_B is Boltzmann's constant. The pressure-dependence data of the dielectric constant of ethanol are given in ref 40. The dielectric constant increases with pressure. Figure 1b shows the static dielectric constant of ethanol at various pressures. The pressure dependence, $\partial\epsilon/\partial P$, decreases as the pressure increases. At 12 kbar, $\epsilon = 33$ as compared with $\epsilon = 24$ at 1 atm and 298 K.

There may be fairly large uncertainty concerning the values of the mutual diffusion constant, D, as a function of pressure. Thus, we face a multi parameter problem in adjusting a solution of a partial differential equation to fit the experimental data.

The asymptotic expression (the long-time behavior) for the fluorescence of ROH*(t) is given by[41]

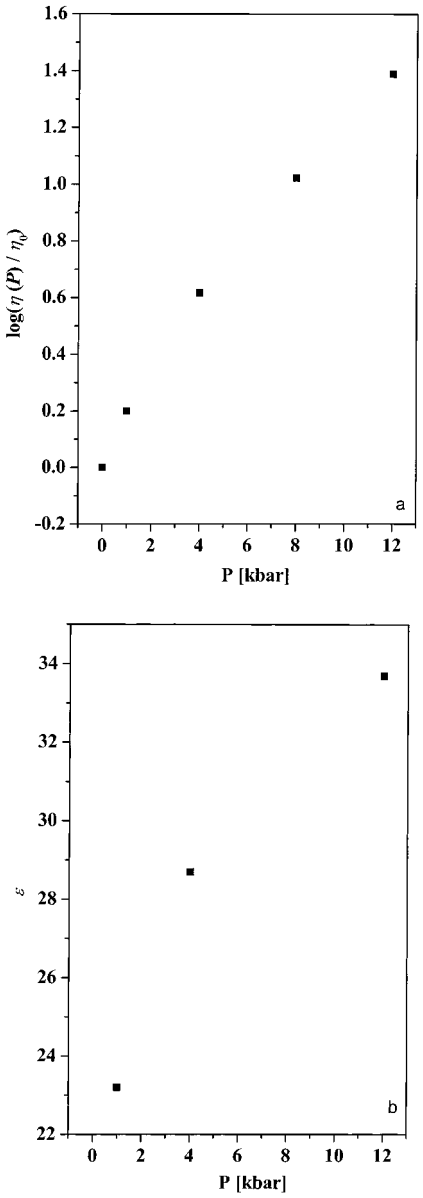

Figure 1. The viscosity dependence on pressure of ethanol (a) at 303 K taken from ref 37 and the static dielectric constant of ethanol (b) at various pressures.

$$[\mathrm{ROH}^*] \cong \frac{\pi}{2} a^2 \exp(R_D/a) \frac{k_r}{k_{PT}(\pi D)^{3/2}} t^{-3/2} \qquad (2)$$

Equation 2 shows that uncertainty in the determination of $D(P)$ causes a larger uncertainty in k_r. Also, the relatively large fluorescence "background", due to a fluorescent impurity in the DCN2 compound and the band overlap, prevents us from accurately determining the recombination rate constant. We estimate that the error in determination of k_{PT} is 10%. The error in the determination of k_{PT} is due to (1) the signal-to-noise ratio of the experimental signal, which affects the quality of the fluorescence signal at longer times, and (2) the interplay between k_{PT} and k_r (see eq 2) over longer times. The uncertainty in the determination of k_r is estimated to be much larger, ~50%. The relatively large uncertainty in the values of k_r arises from the relation between k_r, $D(P)$, and $\epsilon(P)$, where $D(P)$ is estimated and its exact values are unknown. The large background due to the fluorescence of the impurity in the DCN2 sample increases the error in estimating k_r. In this paper, we focus our attention

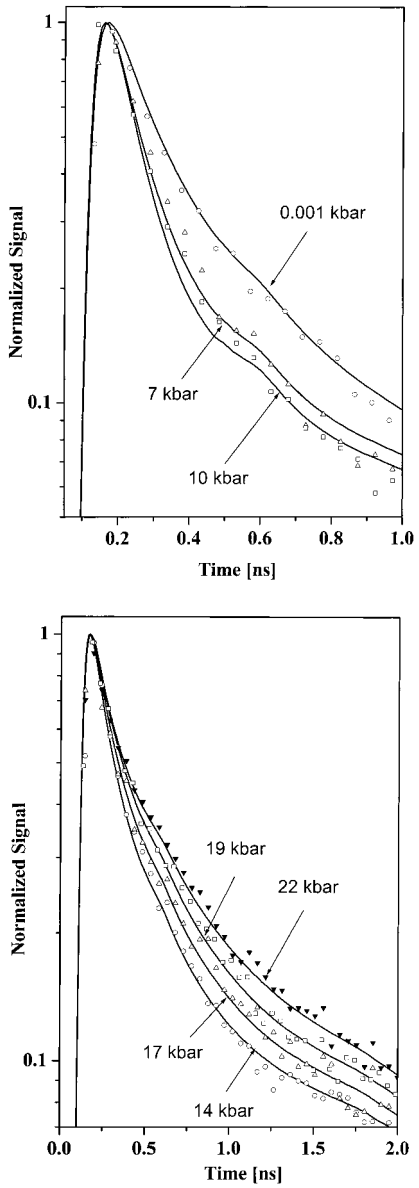

Figure 2. The experimental time-resolved emission intensity data (symbols) of DCN2 in ethanol solution (a) measured at 470 nm at various pressures in the range of 0.001−10 kbar along with the computer fit (solid lines): (○) 0.001 kbar; (△) 7 kbar; (□) 10 kbar. Panel b shows the experimental time-resolved emission intensity data (symbol) of DCN2 in ethanol solution measured at 470 nm at various pressures in the range of 14−22 kbar along with the computer fit (solid lines): (○) 14 kbar; (△) 17 kbar; (□) 19 kbar; (▼) 22 kbar.

on the pressure dependence of the proton-dissociation rate constant, $k_{PT}(P)$, which is measured quite accurately.

Figure 2a shows, on a semilog scale, the experimental time-resolved emission intensity data of DCN2 in an ethanol solution measured at 470 nm at various pressures in the range of 0.001−10 kbar. The experimental data are shown by symbols, and the computer fit is shown by solid lines. We determined the proton-transfer rate constant, k_{PT}, from the fit to the initial fast decay of the ROH* fluorescence (~120 ps for DCN2 in ethanol at 1 atm, $T = 298$ K). The initial fast component of the fluorescence decay is mainly determined by the deprotonation process and is almost insensitive to the geminate recombination process. The long-time behavior (the fluorescence tail) seen in the ROH* time-resolved emission is a consequence of the repopulation of the ROH* species by the reversible recombination of RO^-* with the geminate proton. The reprotonation of the excited ROH*

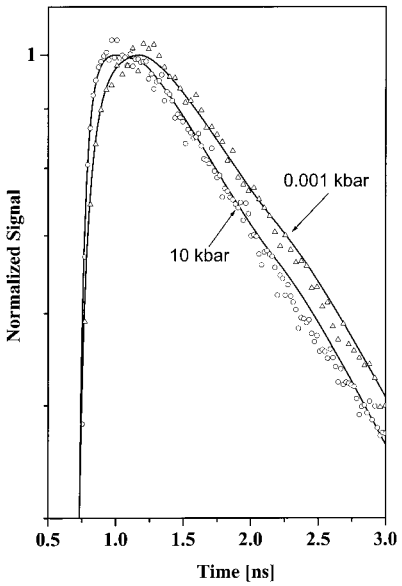

Figure 3. The time-resolved emission of DCN2 RO^-* species in an ethanol solution measured at 650 nm at two pressures in the range 0.001−22 kbar.

can undergo a second cycle of deprotonation. The overall effect is a nonexponential fluorescence tail.[34] As can be seen in the figure, at the pressure range 0.001−10 kbar, the decay rate of the fluorescence increases as the pressure increases. The proton-transfer rate constant, k_{PT}, increases with pressure increase, while the diffusion constant decreases with pressure increase.

Figure 2b shows the fluorescence decay at the high-pressure range, 14−22 kbar. In contrast to the low-pressure range, at the high-pressure range, the proton-transfer rate decreases as the pressure increases.

Figure 3 shows the time-resolved emission of the DCN2 RO^-* species in ethanol solution measured at 650 nm at two pressures in the range of 0.001−22 kbar along with the computer fit (solid line) using the reversible proton-transfer model. The parameters used in the fit are extracted from the fit of the fluorescence decay curves of ROH* species, measured at 450 nm. The emission intensity has a growth time, which corresponds to the proton-transfer rate from the DCN2 ROH species to the solvent. The decay times of the excited-state RO^- are only slightly dependent on the pressure. Table 1 provides a summary of the pressure dependence of the kinetic parameters.

Discussion

The main findings of the experiments are as follows: (1) At relatively low pressures, the proton-transfer rate constant, k_{PT}, increases as the pressure increases. (2) At about 10 kbar, k_{PT} reaches a maximum value, about twice the value at atmospheric pressure. (3) At pressures above 12 kbar, the pressure dependence of k_{PT} decreases with pressure and follows approximately $1/\tau_D$, where τ_D is the slow component of the dielectric relaxation. In ethanol, τ_D decreases as a function of pressure, and hence, the proton-transfer rate at high pressures decreases as a function of pressure.

In the following section, we first present the basic theoretical concepts related to nonadiabatic and adiabatic proton transfers. This will then be followed by a description of our proton-transfer model accounting for the temperature and pressure dependence of the proton-transfer rate. Finally, a correlation of our model of proton transfer with the theory will be presented.

The theory for nonadiabatic proton transfer developed by Kuznetsov and his colleagues[23] is very similar to the theory for

TABLE 1: Pressure Dependence of the Kinetic Parameters for the Proton-Transfer Reaction of DCN2 in Ethanol

P (GPa)[a,b]	k_{PT} (10^9 s^{-1})[c]	k_r (10^9 Å s^{-1})[c,d]	ϵ[e]	D_{H^+} (10^{-4} cm^2 s^{-1})[f]	a_1[g]
0.001	6.5	4.5	24	0.20	0.02
∼0.1	9.0	5.0	26	0.18	0.02
0.35	10.5	5.0	28	0.16	0.023
0.45	11.0	5.0	29	0.14	0.023
0.7	12.5	5.0	32	0.12	0.024
0.85	11.5	5.0	33	0.11	0.026
1	9.5	6.0	34	0.09	0.032
1.4	7.5	6.0	35	0.07	0.032
1.7	6.5	6.0	37	0.06	0.032
1.9	5.8	6.0	38	0.05	0.032
2.2	5.0	6.0	40	0.04	0.034

[a] 1 GPa ≈ 10 kbar. [b] The error in determination of the pressure is ±0.075 GPa. [c] k_{PT} and k_r are obtained from the fit of the experimental data by the reversible proton-transfer model (see text). [d] The error in the determination of k_r is 50% (see text). [e] Data taken from ref 40 up to 12 kbar and extrapolated to higher pressures. [f] Values at high pressure obtained by best fit to the fluorescence decay. [g] Background fluorescence relative amplitude; the lifetime of the background is 10 ns.

nonadiabatic electron transfer in its treatment of the involvement of the solvent. In the model,[23] when the polar solvent is equilibrated to the reactant, the proton will not be transferred because of an energy mismatch in the reactant and product states. Upon a solvent fluctuation, the energy of the reactant and product states becomes equal, and it is in this solvent configuration that the proton tunnels from one side of the well to the other. Finally, upon solvent relaxation, the product state is formed.

If the pretunneling and posttunneling configurations are regarded as real, transient intermediates, the process can be described by a set of chemical equations:[42]

$$AH + S_B + S_R \underset{k_{-1}}{\overset{k_1}{\rightleftharpoons}} AH{\cdot}S_B + S_\ddagger$$

$$AH{\cdot}S_B + S_\ddagger \underset{k_{-2}}{\overset{k_2}{\rightleftharpoons}} A^-{\cdot}HS_B + S_\ddagger$$

$$A^-{\cdot}HS_B + S_\ddagger \xrightarrow{k_3} A^- + HS_B + S_p$$

where AH is the protonated photoacid, S_B is a single solvent molecule to which the proton is transferred, S_R is the solvent configuration to stabilize the reactants, and S_p is the solvent configuration of the products. $S_\ddagger$ is the solvent configuration to equally stabilize $AH{\cdots}S_B$ and $A^-{\cdots}HS_B$.

One important difference between electron transfer and proton transfer is the extreme sensitivity of the proton tunneling matrix element to distance. The functional form of the tunneling coupling matrix element between the reactant and product state, for moderate to weak coupling, is

$$c(Q) = C_0 \exp(-\alpha\delta Q) \qquad (3)$$

The decay parameter α is very large, 25−35 $Å^{-1}$, in comparison with the corresponding decay parameter for the electronic coupling in electron transfer, 1 $Å^{-1}$. In the strong coupling limit, the tunneling matrix element varies much less rapidly with changing Q and is approximately linear. It is this feature that makes the dynamics of proton transfer so sensitive to the internuclear separation of the two heavy atoms. Pressure is used in this study to systematically and gradually change the intermolecular distance.

Kuznetsov[23,24] and Borgis−Hynes[25] introduced a low-frequency vibrational mode, Q, the frequency of which is ω_Q and the associated vibrational reorganization energy of which is E_Q. They derived the nonadiabatic rate constant, k. The tunneling term depends strongly upon a promoting vibration, Q, and the proton-transfer rate increases with respect to a fixed equilibrium distance formula.

A simpler one-dimensional model was used by Bernstein and co-workers to calculate the proton-tunneling rate in gas-phase van der Waals clusters.[2] The model consists of three essential features: (1) the potential-energy barrier is characterized by a width and height, (2) the barrier width and height are modulated by vibrational excitation of the intermolecular cluster modes, and (3) vibrational energy is distributed statistically among the vibrational (van der Waals) modes. Tunneling rates can be calculated as a function of the heavy atom separation based upon the WKB approximation for particle penetration through a barrier of assumed functional form.

Calculations of the proton-transfer rate of this simple model reveal that the stretching mode has a profound effect on the proton-transfer rate. For a parabolic barrier shape and a barrier height of 8000 cm^{-1} and half width of 0.2 Å, and intermolecular vibrational frequency of $\sim$120 cm^{-1}, the tunneling rate increases by more than 3 orders of magnitude from 10^8 to 10^{11} s^{-1}.

A Qualitative Model for the Temperature and Pressure Dependencies of Excited-State Proton-Transfer Reactions. Previously, we used a qualitative model that accounts for the unusual temperature dependence of the excited-state proton transfer.[14,15] We will use the same model to explain the pressure results. The proton-transfer reaction depends on two coordinates; the first one depends on a generalized solvent configuration. The solvent-coordinate characteristic time is within the range of the dielectric relaxation time, τ_D, and the longitudinal relaxation, $\tau_L = (\epsilon_0/\epsilon_s)\tau_D$. The second coordinate is the actual proton translational motion (tunneling) along the reaction path.

The model restricts the proton-transfer process to be stepwise. The proton moves to the adjacent hydrogen-bonded solvent molecule only when the solvent configuration brings the system to the crossing point according to the Kuznetsov model.[23] In the stepwise model, the overall proton-transfer time is the sum of two times, $\tau = \tau_1 + \tau_2$, where τ_1 is the characteristic time for the solvent reorganization and τ_2 is the time for the proton to pass to the acceptor. The overall temperature- and pressure-dependent rate constant, $k_{PT}(T,P)$, at a given T and P is

$$k_{PT}(T,P) = \frac{k_H(T,P)k_S(T,P)}{k_H(T,P) + k_S(T,P)} \tag{4}$$

where k_S is the solvent coordinate rate constant and k_H is the proton coordinate rate constant.

Equation 4 provides the overall excited-state proton-transfer rate constant along the lines of a stepwise process similar to the processes mentioned above. As a solvent coordinate rate constant, we use $k_S(T,P) = b(1/\tau_D)$, where b is an adjustable empirical factor determined from the computer fit of the experimental data. We find that the empirical factor for monols lies between 2 and 4. For the monols, τ_L is usually smaller than τ_D by a factor of 2−6. Thus, the solvent characteristic time, $\tau_S = 1/k_S(T,P)$, for monols lies between the dielectric relaxation and the longitudinal time, $\tau_L < \tau_S < \tau_D$. The reaction rate constant, k_H, along the proton coordinate is expressed by the usual activated chemical reaction description given by eq 5. At high temperatures, the solvent relaxation is fast and the rate-determining step is the actual proton-transfer coordinate.

$$k_H = k_H^0(P)\exp\left(-\frac{\Delta G^{\ddagger}}{RT}\right) \tag{5}$$

where k_H^0 is the preexponential factor determined by the fit to the experimental results and $\Delta G^{\ddagger}$ is the activation energy. The activation energy, $\Delta G^{\ddagger}$, is determined from the excited-state acid equilibrium constant, K_a^*, and the structure reactivity relation of Agmon and Levin.[43] For DCN2, pK^* = −4.5, we find for ethanol solution $\Delta G^{\ddagger}$ = 2 kJ/mol.

The effect of pressure and temperature on the photoinduced hydrogen-transfer reaction in a mixed crystal of acridine in fluorene was studied by Bromberg et al.[44] The room-temperature hydrogen-transfer rate increases exponentially with increasing the pressure. Trakhtenberg and Klochikhin[8] derived an expression for the pressure and temperature dependence of the tunneling rate of proton transfer in the solid state:

$$k(P,T) = \nu\exp[-J(R_0) + J'R_0(1-\alpha^{-1/3}) + J'^2\delta_{CN}{}^2/(8\alpha^{\gamma}) \times \coth(\hbar\Omega_0\alpha^{\gamma}/(4k_BT))] \tag{6}$$

where $\alpha(P) = V_0/V(P)$, Ω_p is the effective frequency of the intermolecular vibration, $\delta_{CN}{}^2$ is the square of the amplitude of the intercenter C···N distance, and $\gamma = -\partial \ln \Omega_p/(\partial \ln V)$.

$$J(R) = (2/\hbar)\int\{2m[U(x,R) - E_H(R)]\}^{1/2}\,dx \tag{7}$$

$E_H(R)$ and $U(x,R)$ are the total and the potential energy of the tunneling atom, respectively, depending on the distance R between the two heavy atoms (in our case two oxygen atoms). R_0 is the equilibrium distance between the heavy atoms and J' is the derivative $\partial J/\partial R$. Trakhtenberg et al.[8] found good correspondence with the experimental results of Bromberg et al.[44] when they used a smaller power dependence of the compressibility α (0.22 instead of $^1/_3$).

We estimated the pressure dependence of the proton coordinate rate constant, $k_H(P)$, from the second term of eq 6 with a compressibility dependence on power of 0.22.

$$\frac{k_H(P)}{k_H(1\text{ atm})} \cong \exp[J'R_0(1-\alpha^{-0.22})] \tag{8}$$

In our treatment, we neglect the contribution to the pressure dependence of the rate constant of the third term in eq 6, which we estimate to be smaller.

Figure 4 shows the dependence of $1/\alpha = V_P/V_0$ on the pressure, where V_P is taken from ref 37. The compressibility, $1/V(\partial V/\partial P)_T$, is a function of P. In most alcohols, and in many liquids, the change in volume with pressure at a pressure range up to 12 kbar is quite the same, $V_P/V_0 \cong 0.75$. The compressibility decreases with pressure. It changes by about a factor of 10 between atmospheric pressure and 12 kbar. Figure 5 shows the pressure dependence of the proton tunneling rate constant, using eq 8, and the following parameters: $J' = 25$ Å^{-1}, $R_0 = 2.4$ Å, and α taken from ref 37. As can be seen, the rate increases as a function of pressure. Because $1/\alpha$ is not constant with pressure but decreases as the pressure increases, so too $k_H(P)/k_H(1\text{ atm})$ does not increase with the same initial slope. At 20 kbar, k_H only increases slightly with the pressure increase.

In previous studies,[14−17] we used the longest component of the dielectric relaxation time, τ_D, for the solvent coordinate rate constant, $k_S = b/\tau_D$, where b is an empirical factor. For all monols studied, $2 < b < 4$. We are not aware of literature-published values of the dielectric relaxation times as a function of pressure for ethanol. In many cases, the viscosity and τ_D have

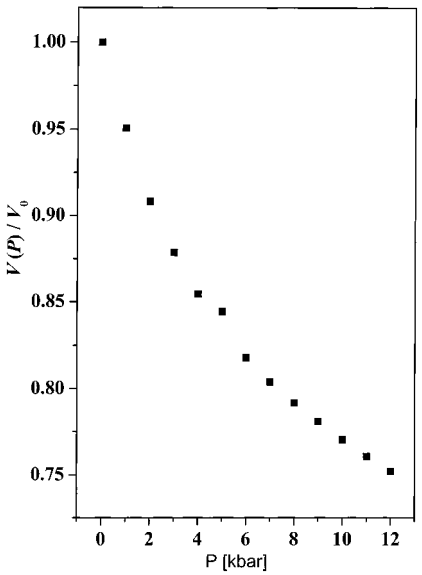

Figure 4. The pressure dependence of $1/\alpha = V_P/V_0$ of ethanol.

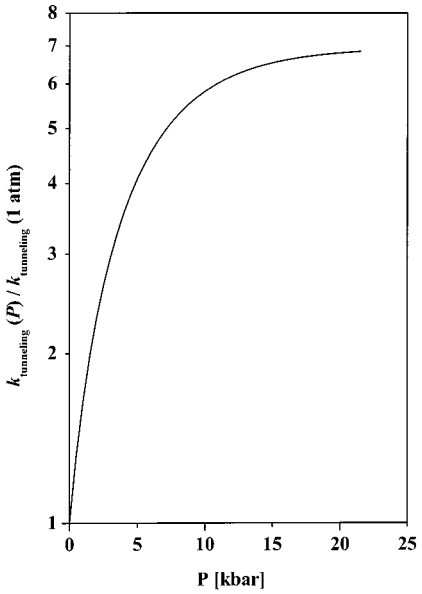

Figure 5. The pressure dependence of the proton-tunneling rate constant, using eq 8. The parameter $J' = 25$ Å^{-1}, $R_0 = 2.4$ Å, and α was taken from ref 37.

similar dependencies on both pressure and temperature. The dielectric relaxation time is often directly proportional to the shear viscosity. This is a direct consequence of the assumed viscous-damped rotating sphere model of dielectric relaxation originally introduced by Debye.[45]

Johari and Danhauser studied the pressure dependence of the dielectric relaxation of isomeric octanols.[46] The dielectric relaxation time, τ_D, of isomeric octanols decreases with pressure increase in the range of 0.001−4 kbar. The pressure dependence of τ_D of 2-methyl-3-heptanol is close to exponential at the temperature range of 215−250 K. At 250 K, τ_D increases by about 3 orders of magnitude by increasing the pressure to 4 kbar. For 3-octanol, τ_D exhibits a nonexponential behavior as a function of pressure. The slope, $(\partial \ln \tau_D/\partial P)_T$, decreases as the pressure increases. Johari and Danhauser also studied the viscosity dependence of isomeric octanols[47] and compared it with the dielectric relaxation pressure dependence. They found good correspondence between the pressure dependence of the

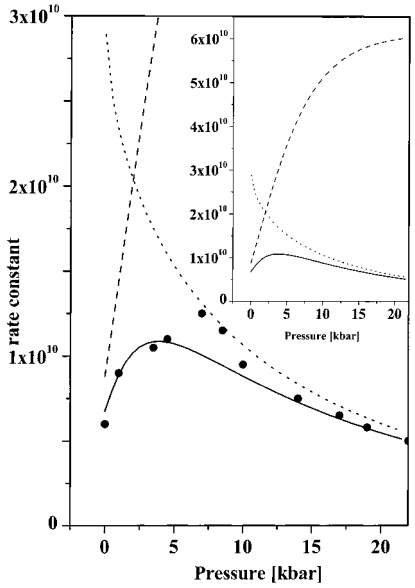

Figure 6. A fit to the stepwise two-coordinate model of $k_{PT}(P) = k_H(P)k_S(P)/(k_H(P) + k_S(P))$ as a function of pressure (solid line) along with the experimental data (dots). $k_H(P)$ and $k_S(P)$ are shown as dashed and dotted lines, respectively. The inset shows an extended vertical scale.

viscosity and dielectric relaxation times. In general, the viscosity dependence on pressure is larger than that of the dielectric relaxation.

Figure 1a shows the viscosity dependence on pressure of ethanol at 303 K, taken from ref 37. We used an approximate relation between $\tau_D(P)$ and $\eta(P)$ based on the correspondence between dielectric relaxation and $\eta(P)$ to estimate the pressure dependence of the $\tau_D(P)$ of ethanol.

$$\tau_D(P) \approx \tau_D^{1atm}\left(\frac{\eta(P)}{\eta^{1atm}}\right)^{\delta} \tag{9}$$

For best fit to the pressure dependence of k_{PT} using our stepwise model, we used $\delta = 0.7$.

Figure 6 shows a fit to the stepwise two-coordinate model of $k_{PT}(P) = k_H(P)k_S(P)/(k_H(P) + k_S(P))$ as a function of pressure (solid line) along with the experimental data (dots). The results show first a fast increase of the rate with the pressure. At about 8 kbar, the rate reaches a maximum value, $k_{PT}(8\text{ kbar}) = 2k_{PT}(1\text{ atm})$. Further increase of the pressure decreases the rate constant of the proton transfer to the solvent. This interesting observation of the pressure dependence is explained by the opposite pressure dependencies of k_H and k_S and the saturation of k_H at medium-pressure values. The pressure dependence of k_H and k_S are also plotted (dotted lines) in Figure 6.

Qualitative Comparison of the Pressure Dependence of Proton Transfer with the Landau−Zener Curve-Crossing Formulation. In this section, we will compare our qualitative model based on the pressure and temperature dependences of the proton-transfer rate with the Landau−Zener curve-crossing formulation. The reaction can be described schematically:

$$A^*H\cdots S_B \rightarrow A^{-}{}^*\cdots HS_B^{+} \tag{10}$$

The reactant is an intermolecular hydrogen-bonded complex between the photoacid, AH*, and a solvent molecule, S_B, that serves as a base, characterized by a hydrogen bond to the photoacid and also other solvent molecules. In water, this specific water molecule, S_B, has three hydrogen bonds to three

water molecules. To form the product, $A\cdots HS_B^+$, in water, one hydrogen bond, of S_B to a water molecule, must break. Thus, relatively long-range reorganization of the hydrogen-bond network takes place upon proton transfer to the solvent. This complex rearrangement, to accommodate the product, is probably the reason for a slow solvent-generalized configuration motion, which corresponds to a low-frequency component in the solvent dielectric spectrum. Its time constant is close to the slow component of the dielectric relaxation time. According to Kuznetsov,[23] Borgis and Hynes,[25] Bernstein and co-workers,[2] Syage,[4] and Trakhtenberg,[8,9] a second important coordinate should be taken into account. This second coordinate is the distance between the two heavy atoms, O—H···O in our case. This distance is modulated by a low-frequency vibrational mode, *Q*.[2,25] The proton tunnels through the barrier from the reactant well to the product well via the assistance of the low-frequency, *Q*, mode whenever the solvent configuration equalizes the energies of the reactant and the product. Free-energy relation[48,49] and the temperature-dependence experiments[16] indicate that the solvent fluctuation rate to equalize the energies is not of the order of 10^{13} s^{-1} but slower than 10^{12} s^{-1}. For monols, diols, and glycerol, it is very close to $1/\tau_D$, where τ_D is the slow component of the dielectric relaxation time.

Borgis and Hynes[25] derived an expression for the rate constant, *k*, for a proton transfer between the reactant and the product. The constant *k* can be expressed as the average one-way flux in the solvent coordinate through the crossing point, *S**, of the two free-energy curves with the inclusion of the transmission coefficient, κ, giving the probability of a successful curve crossing:

$$k = \langle \dot{S}\Theta(\dot{S})\delta(S - S^*)\kappa(\dot{S},S^*)\rangle_R \tag{11}$$

where *S* is the solvent coordinate, $\dot{S}$ is the solvent velocity, and $\Theta(\dot{S})$ is the positive velocity step function. Here, the average is over the classical solvent distribution, normalized by the partition function of the solvent in the reactant region.

The LZ factor, appropriate for a positive velocity approach to the crossing point, is

$$\kappa = [1 - {}^1/_2 \exp(-\gamma)]^{-1}[1 - \exp(-\gamma)] \tag{12}$$

$$\gamma = \frac{2\pi C^2}{\hbar(\partial\Delta V/\partial S)_{S^*}\dot{S}} = \frac{2\pi C^2}{\hbar k_{S^*}\dot{S}} \tag{13}$$

κ includes multiple-pass effects on the transition probability. (Note that $\kappa \rightarrow 1$ is the adiabatic limit). When $\gamma \ll 1$, one obtains the nonadiabatic limit result

$$\kappa = 2\gamma \tag{14}$$

This leads to

$$k = \frac{2\pi}{\hbar}C^2\left[\left(\frac{\beta}{4E_S\pi}\right)^{1/2} e^{-\beta\Delta G^{\ddagger}}\right] \tag{15}$$

in which $\Delta G^{\ddagger}$ is the activation free energy

$$\Delta G^{\ddagger} = \frac{1}{4E_S}(E_S + \Delta G + \Delta E)^2 \tag{16}$$

γ (see eq 13) depends on the potential surfaces curvature, $(\partial\Delta V/\partial S)_{S^*}$, on C^2 and on $\dot{S}$. C^2 depends strongly on pressure via the internuclear distance, and the *Q* intermolecular vibrational mode depends to a lesser extent on pressure. The solvent velocity, $\dot{S}$, depends strongly both on the temperature and on the pressure. In fact, $\dot{S}$ relates to the solvent relaxation. On the basis of the experimental data and the qualitative stepwise model of the pressure and temperature dependence of the rate constant of the proton transfer, we infer that $\dot{S} = b/\tau_D$, where τ_D is the solvent dielectric relaxation time and *b* is a factor between 2 and 4 for monols.

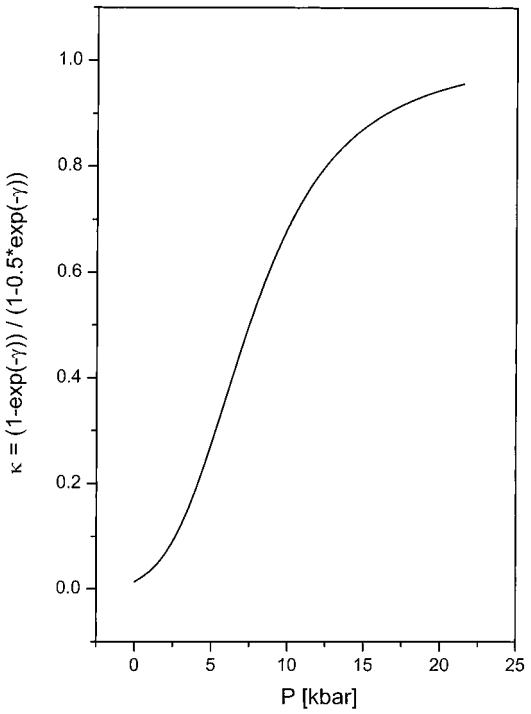

Figure 7. The pressure dependence of the transmission coefficient, κ, for an ethanol solution as a function of pressure.

For the solvents used in the experiments of ref 16, the value of γ as a function of the temperature smoothly increases from a value close to 0, that is, $\gamma \ll 1$ (the nonadiabatic limit), to a value of $\gamma \gg 1$ (the adiabatic limit). An illustration of the pressure dependence of the transmission coefficient, κ, for proton transfer from DCN2 ROH* species to ethanol solution is shown in Figure 7. We used eqs 12 and 13, and we assume that the pressure dependence of the coupling matrix element can be given by

$$C = C_0 \exp[J'R_0(1 - \alpha^{-0.22})] \tag{17}$$

Equation 17 is similar to eq 3 and uses the second term of Trakhtenberg's pressure dependence of the proton-tunneling rate. In Figure 7, we used $2\pi C_0^2/(\hbar k_{S^*}) = 2 \times 10^8$. It is clearly seen that the transmission coefficient, κ, changes from close to zero at low pressure to close to 1 at high pressure.

Rips and Jortner[50] derived an expression for the electron-transfer (ET) rate that bridges between the nonadiabatic and the solvent-controlled adiabatic limit. The expression for the overall ET rate constant that they derived is

$$k_{ET}{}^{-1} = (k_{ET}^{NA})^{-1} + (k_{ET}^{AD})^{-1} = \tau_{ET}^{AD} + \tau_{ET}^{NA} \tag{18}$$

$$k_{ET} = \frac{k_{ET}^{NA}k_{ET}^{AD}}{k_{ET}^{NA} + k_{ET}^{AD}} \tag{19}$$

where k_{ET}^{AD} and k_{ET}^{NA} are the adiabatic and nonadiabatic rate constants, respectively. These rate constants have a similar functional form to the proton-transfer rates given by Borgis and Hynes.[25]

Our stepwise model[15−17] is similar to the expression of Rips and Jortner[50] for the overall ET rate constant that bridges between the two extreme cases, the nonadiabatic and the adiabatic ET. The expression that bridges between the nonadiabatic and the solvent-controlled adiabatic limit for the proton transfer to the solvent is

$$k_{PT}(T,P) = \frac{k_{PT}^{NA}(T,P)k_{PT}^{AD}(T,P)}{k_{PT}^{NA}(T,P) + k_{PT}^{AD}(T,P)} \quad (20)$$

To use the rate constants quantitatively, we face some unknown parameters. The rate constant for the nonadiabatic proton transfer includes the unknown coupling matrix, *C*. We do not know the absolute value of the coupling matrix element, but we can formulate (eq 17) the pressure dependence and use the classical Arrhenius expression for the pressure dependence of the nonadiabatic rate constant

$$k_{PT}^{NA} = k_0(P)\exp(-\beta\Delta G_{NA}^{\ddagger}) \quad (21)$$

$$k_0(P) = k_0(1\text{ atm})\exp[-J'R_0(1-\alpha^{-0.22})] \quad (22)$$

For the adiabatic limit, Borgis and Hynes found[25] that

$$k_{PT}^{AD} = \left(\frac{\omega_S}{2\pi}\right)\exp(-\beta\Delta G_{AD}^{\ddagger}) \quad (23)$$

The formal expressions for the pressure dependence of k_{PT}^{NA} and k_{PT}^{AD} are given by eqs 22 and 23. k_{PT}^{NA} is qualitatively parallel to k_H in eq 4. Accordingly, the prefactor, k_H^0, depends on the pressure. k_{PT}^{AD} is similar to k_S in eq 4. The time scale of the solvent control is slow and close to τ_D. Using eq 20 to calculate $k_{PT}(T,P)$ as a function of the pressure results in qualitatively similar behavior to eq 4. Figure 6 shows such a fit to the experimental data. As can be seen, the fit is good. The tunneling rate constant, k_{PT}^{NA}, increases with pressure from atmospheric pressure to 20 kbar by a factor of 8, while the solvent-controlled adiabatic rate constant, k_{PT}^{AD} , decreases with pressure by a factor of 4. The total rate $k_{PT}(T,P)$ first increases with pressure by a factor of 2, and at high pressure, it decreases as the solvent controls the overall rate.

Summary

We have studied by time-resolved emission techniques the proton dissociation and the reversible geminate recombination processes as a function of pressure in ethanol. DCN2 is used as the excited-state proton emitter (photoacid). The experimental time-resolved fluorescence data are analyzed by the exact numerical solution of the transient Debye−Smoluchowski equation (DSE).

We have found that the proton-dissociation rate constant, k_{PT}, of excited DCN2 in neat ethanol at relatively low pressure (up to 10 kbar) increases with pressure, while at higher pressure up to the freezing point, the proton-transfer rate decreases with pressure and its value is similar to the inverse of the dielectric relaxation time.

We used a stepwise model to qualitatively fit the pressure dependence of the proton-transfer rate. The analysis of the experimental data by the model shows that the pressure affects both steps but in the opposite direction. The tunneling rate increases with pressure, while the solvent relaxation decreases with pressure.

Acknowledgment. We thank Prof. L. Tolbert for providing the 5,8-dicyano-2-naphthol. We thank Prof. M. Pasternak and Dr. G. Rozenberg for providing the diamond anvil cell high-pressure technology. This work was supported by grants from the US-Israel Binational Science Foundation and the James-Franck German-Israel Program in Laser-Matter Interaction.

References and Notes

(1) Knochenmuss, R. *Chem. Phys. Lett.* **1998**, *293*, 191.
(2) Hineman, M. F.; Brucker, G. A.; Kelley, D. F.; Bernstein, E. R. *J. Chem. Phys.* **1992**, *97*, 3341.
(3) Peters, K. S.; Cashin, A.; Timbers, P. *J. Am. Chem. Soc.* **2000**, *122*, 107.
(4) Syage, J. A. *J. Phys. Chem.* **1995**, *99*, 5772.
(5) Rollinson, A. M.; Drickamer, H. G. *J. Chem. Phys.* **1980,** *73*, 5981.
(6) Chan, I. Y.; Dernis, M. S.; Wong, C. M.; Stehlik, D. *J. Chem. Phys.* **1995**, *103*, 2959.
(7) Sumi, H.; Asano, T. J. *J. Chem Phys.* **1995**, *102*, 9565.
(8) Trakhtenberg, L. I.; Klochikhin, V. L. *Chem. Phys.* **1998**, *232*, 175.
(9) Goldanskii, V. I.; Trakhtenberg, L. I.; Fleuorov, V. N. *Tunneling Phenomena in Chemical Physics*; Gordon and Breach: New York, 1989; Chapter IV.
(10) Ireland, J. F.; Wyatt, P. A. H. *Adv. Phys. Org. Chem.* **1976**, *12*, 131.
(11) Huppert, D.; Gutman, M.; Kaufmann, K. J. In *Advances in Chemical Physics*; Jortner, J., Levine, R. D., Rice, S. A., Eds.; Wiley: New York, 1981; Vol. 47, p 681. Koswer, E.; Huppert, D. In *Annual Reviews of Physical Chemistry*; Strauss, H. L., Babcok, G. T., Moore, C. B., Eds.; Annual Reviews Inc: Palo Alto, CA, 1986; Vol 47, p 122.
(12) Lee, J.; Robinson, G. W.; Webb, S. P.; Philips, L. A.; Clark, J. H. *J. Am. Chem. Soc.* **1986**, *108*, 6538.
(13) Gutman, M.; Nachliel, E. *Biochim. Biophys. Acta* **1990**, *391*, 1015.
(14) Poles, E.; Cohen, B.; Huppert, D. *Isr. J. Chem.* **1999**, *39*, 347.
(15) Cohen, B.; Huppert, D. *J. Phys. Chem. A* **2000**, *104*, 2663.
(16) Cohen, B.; Huppert, D. *J. Phys. Chem. A* **2001**, *105*, 2980.
(17) Cohen, B.; Huppert, D. *J. Phys. Chem. A* **2002**, *106*, 1946.
(18) Kolodney, E.; Huppert, D. *J. Chem. Phys.* **1981**, *63*, 401.
(19) Ando, K.; Hynes, J. T. In *Structure, energetics and reactivity in aqueous solution*; Cramer, C. J., Truhlar, D. G., Eds.; American Chemical Society: Washington, DC, 1994.
(20) Agmon, N.; Huppert, D.; Masad, A.; Pines, E. *J. Phys. Chem.* **1991**, *96*, 952.
(21) Bell, R. P. *The Tunnel Effect in Chemistry*; Chapman and Hall: London, 1980.
(22) Bell, R. P. *The Proton in Chemistry*; Chapman and Hall: London, 1973.
(23) German, E. D.; Kuznetsov, A. M.; Dogonadze, R. R. *J. Chem. Soc., Faraday Trans. 2* **1980**, *76*, 1128.
(24) Kuznetsov, A. M. *Charge Transfer in Physics, Chemistry and Biology*; Gordon and Breach: Amsterdam, 1995.
(25) Borgis, D.; Hynes, J. T. *J. Phys. Chem.* **1996**, *100*, 1118. Borgis, D. C.; Lee, S.; Hynes, J. T. *Chem. Phys. Lett.* **1989**, *162*, 19. Borgis, D.; Hynes, J. T. *J. Chem. Phys.* **1991**, *94*, 3619.
(26) Cukier, R. I.; Morillo, M. *J. Chem. Phys.* **1989**, *91*, 857. Morillo, M.; Cukier, R. I. *J. Chem. Phys.* **1990**, *92*, 4833.
(27) Li, D.; Voth, G. A. *J. Phys. Chem.* **1991**, *95*, 10425. Lobaugh, J.; Voth, G. A. *J. Chem. Phys.* **1994**, *100*, 3039.
(28) Huppert, D.; Jayaraman, A.; Maines, R. G., Sr.; Steyert, D. W.; Rentzepis, P. M. *J. Chem. Phys.* **1984**, *81*, 5596.
(29) Jayaraman, A. *Rev. Mod. Phys.* **1983**, *55*, 65.
(30) Machavariani, G. Yu.; Pasternak, M. P.; Hearne, G. R.; Rozenberg, G. Kh. *Rev. Sci. Instrum.* **1998**, *69*, 1423.
(31) D′ANVILS is administered by Ramot Ltd., 32 H. Levanon Str., Tel Aviv 61392, Israel. http://www.tau.ac.il/ramot/danvils.
(32) Barnett, J. D.; Block, S.; Piermarini, G. J. *Rev. Sci. Instrum.* **1973**, *44*, 1.
(33) Tolbert, L. M.; Haubrich, J. E. *J. Am. Chem. Soc.* **1990**, *112*, 8163. Tolbert, L. M.; Haubrich, J. E. *J. Am. Chem. Soc.* **1994**, *116*, 10593.
(34) Pines, E.; Huppert, D.; Agmon, N. *J. Chem. Phys.* **1988**, *88*, 5620.
(35) Agmon, N.; Pines, E.; Huppert, D. *J. Chem. Phys.* **1988**, *88*, 5631.
(36) Debye, P. *Trans. Electrochem. Soc.* **1942**, *82*, 265.
(37) Bridgman, P. E. *The Physics of High Pressure*; G. Bell and Sons Ltd: London, 1958.
(38) Erdey-Gruz, T.; Lengyel, S. In *Modern Aspects of Electrochemistry*; Bockris, J. O'M., Conway, B. E., Eds.; Plenum: New York, 1964; Vol. 12, pp 1−40.
(39) Andrussow, L.; Schramm, B. In Schaffer, K., Ed.; Landolt-Bornstein, Vol. 2; Springer: Berlin, 1969.

(40) Smyth, C. P. *Dielectric Behavior and Structure*; McGraw-Hill Book Co.: New York, 1955.
(41) Agmon, N.; Goldberg, S. Y.; Huppert, D. *J. Mol. Liq.* **1995**, *64*, 161.
(42) Kreevoy, M. M.; Kotchevar, A. T. *J. Am. Chem. Soc.* **1990**, *112*, 3579. Kotchevar, A. T.; Kreevoy, M. M. *J. Phys. Chem.* **1991**, *95*, 10345.
(43) Agmon, N.; Levine, R. D. *Chem. Phys. Lett.* **1977**, *52*, 197. Agmon, N.; Levine, R. D. *Isr. J. Chem.* **1980**, *19*, 330.
(44) Bromberg, S.; Chan, I.; Schilke, D.; Stehlik, D. *J. Chem. Phys.* **1993**, *98*, 6284.
(45) Smyth, C. P. *Dielectric Behavior and Structure*; McGraw-Hill Book Co: New York, 1955; p 114.
(46) Johari, G.; Dannhauser, W. *J. Chem. Phys.* **1969**, *50*, 1862.
(47) Johari, G.; Dannhauser, W. *J. Chem. Phys.* **1969**, *51*, 1626.
(48) Pines, E.; Fleming, G. R. *Chem. Phys. Lett.* **1994**, *183*, 393. Pines, E.; Magnes, B.; Lang, M. J.; Fleming, G. R. *Chem. Phys. Lett.* **1997**, *281*, 413.
(49) Solntsev, K.; Huppert, D.; Agmon, N. *J. Phys. Chem. A* **2000**, *104*, 4658.
(50) Rips, I.; Jortner, J. *J. Chem. Phys.* **1987**, *87*, 2090.